

Deep Learning for Real Time Satellite Pose Estimation on Low Power Edge TPU

Alessandro Lotti, Dario Modenini, *Member, IEEE*, Paolo Tortora, *Senior Member, IEEE*,
Massimiliano Saponara, and Maria A. Perino

Abstract— Pose estimation of an uncooperative space resident object is a key asset towards autonomy in close proximity operations. In this context monocular cameras are a valuable solution because of their low system requirements. However, the associated image processing algorithms are either too computationally expensive for real time on-board implementation, or not enough accurate. In this paper we propose a pose estimation software exploiting neural network architectures which can be scaled to different accuracy-latency trade-offs. We designed our pipeline to be compatible with Edge Tensor Processing Units to show how low power machine learning accelerators could enable Artificial Intelligence exploitation in space. The neural networks were tested both on the benchmark Spacecraft Pose Estimation Dataset, and on the purposely developed Cosmo Photorealistic Dataset, which depicts a COSMO-SkyMed satellite in a variety of random poses and steerable solar panels orientations. The lightest version of our architecture achieves state-of-the-art accuracy on both datasets but at a fraction of networks complexity, running at 7.7 frames per second on a Coral Dev Board Mini consuming just 2.2W.

Index Terms— Satellites, artificial intelligence, neural network applications, machine vision

I. INTRODUCTION

On-orbit Servicing (OOS) and Active Debris Removal (ADR) represent a new frontier for the space economy. On one side, the need to de-orbit the debris that pose a threat to operating satellites is widely recognized to guarantee continuous and safe access to space. On the other side, OOS operations could result in a cost containment with respect to full replacement. In these mission scenarios, the servicing probes are required to maneuver in close proximity with high autonomy, which is an extremely critical task owing to the risk of collision. Guidance and control laws shall be fed with information on the relative chaser-to-target pose (i.e. position and attitude). Additionally, when the target is non-cooperative the

A. Lotti is with the Department of Industrial Engineering, Alma Mater Studiorum Università di Bologna, Forlì, 47121, Italy (e-mail: alessandro.lotti@unibo.it).

D. Modenini, and P. Tortora are with the Department of Industrial Engineering and with the Interdepartmental Centre for Industrial Research, Alma Mater Studiorum Università di Bologna, Forlì, 47121, Italy (e-mail: {dario.modenini, paolo.tortora}@unibo.it).

M. Saponara and M. A. Perino are with Thales Alenia Space Italia, Turin, 10146, Italy (e-mail: {massimiliano.saponara, mariaantonietta.perino}@thalesaleniaspace.com}).

This work was supported by Thales Alenia Space Italia, in the framework of the project “A testbed for deep learning in support of docking-grasping operations”.

relative pose must be estimated autonomously by the chaser. To this aim, vision based navigation through a monocular camera is a viable solution as these sensors are simple, light, and consume little power. However, their adoption is challenged by some inherent limitations of Image Processing (IP) algorithms. Those can be divided in i) hand-crafted features, and ii) deep learning based. The former are affected by low robustness against typical space imagery characteristics such as low Signal-to-Noise-Ratio (SNR), severe, and rapidly varying illumination conditions, and backgrounds. Deep Learning (DL) algorithms could overcome such weaknesses through proper training but present other challenges, namely the need of large datasets, that are difficult to collect for space targets, and a scarce accuracy-computational burden trade-off which prevents real time inference on typical low power on-board computers. A possible solution may be found in the power efficient and high performing co-processors for Machine Learning (ML) at the edge that are being developed for terrestrial applications [1].

Indeed, in recent years deep learning has been shown to aid spacecraft monocular pose estimation at different levels. Sharma *et al* [2] addressed the problem as a classification task by discretizing the pose space and training a Neural Network (NN) to identify the nearest one. Later, Sharma and D’Amico [3], proposed a solution based on joint classification and regression, leveraging an object detector and a Gauss-Newton algorithm for position assessment. In this last work, the authors also presented the Spacecraft PosE Estimation Dataset (SPEED), providing synthetic and real images of the Tango spacecraft. SPEED has been employed as a benchmark during the first Satellite Pose Estimation Challenge (SPEC) [4] hosted by the European Space Agency’s Advanced Concept Team. The competition allowed to move the state-of-the-art forward and provided useful insights for further research. Three out the four top-scoring works exploited Convolutional Neural Networks (CNNs) to detect the target on the image, and to regress the locations of some predefined keypoints, which are then fed into off-the-shelf Perspective-n-Point (PnP) solvers [5]-[6]. On the other hand, the third classified [7] proposed an end to end CNN based pipeline. Since submissions were ranked solely on their average normalized position and quaternion rotation error, regardless of their computational burden, the top-ranked teams relied on extremely large NN models and images resolution, not suitable for real-time spaceborne inference. Only the Stanford’s Space Rendezvous Laboratory (SLAB) baseline solution addressed this issue by replacing traditional convolutions with depthwise separable convolutions.

Inspired by the SPEC results, Black *et al.* [8] proposed a light pipeline able to run at 6.6 frames per seconds (fps) on an

Intel Joule 570x board. The work would have ranked third with however a significant gap from the two top submissions.

More recently, Hu *et al.* [9] proposed a single stage network leveraging a 3D loss to make the pose error less sensitive to depth variations. Their results reach the state-of-the-art, upon a pose refinement step. However, the large image size and the high number of networks' parameters, may undermine embedded real-time inference.

In this context, our work tackles the pose estimation accuracy-latency trade-off from two perspectives. First, we propose a three stage pipeline based on modern neural networks with an architecture that can be easily scaled to the available computational power. Second, we investigate the effect of optimization through quantization. The lightest, optimized version of our pipeline reaches state-of-the-art accuracy and real time inference on the Coral Dev Board Mini 1.5 GHz quadcore CPU, leveraging shallow networks and a contained memory footprint. Finally, we illustrate how Edge Tensor Processing Unit (TPU) devices can further reduce latency, enabling real time inference at extremely low power levels making them suitable candidates for next generation of Artificial Intelligence (AI) enabled satellites. Our algorithms are tested on the Spacecraft Pose Estimation Dataset (SPEED) and on the Cosmo Photorealistic Dataset (CPD), developed as part of this work, depicting a Cosmo SkyMed satellite in heterogeneous combinations of poses, physical configurations, lighting conditions, and backgrounds.

II. COSMO PHOTOREALISTIC DATASET

To the best of the authors' knowledge, none of the datasets developed as part of the works reviewed in Section I includes moving components. However, those are common for large spacecrafts, i.e. the ones that would benefit the most from OOS, which are often equipped with movable antennas and solar arrays. The need to validate pose estimation pipelines even in this scenario, drove the design of a new dataset, named Cosmo Photorealistic Dataset (CPD), depicting a satellite from the SkyMed Earth observation constellation. To this end, the 3D computer graphics software Blender was selected because of its native support to Physically Based Rendering (PBR). Most assumptions adopted for setting the spacecraft pose distribution and image post-processing follow that of SPEED dataset for ease of benchmarking, as detailed in the following.

A. Blender Scene

The Blender scene consists of three concentric highly polygonal spheres representing Earth, clouds, and atmosphere plus a CAD model of the COSMO spacecraft. Similarly to [7], the Earth was textured with a high resolution albedo map further augmented with an ocean mask¹ and topography data from the NASA's Blue Marble collection² which also provided clouds texture. A third-party shader³ was applied to increase the realism of the clouds providing at the same time transparency, diffusion, and reflection. Atmospheric scattering was emulated exploiting Blender's volumetric rendering in

combination with a second shader, from the same package, which implements an exponential density model.

A Blender's sun lamp emulates the Sun by providing collimated light at a blackbody temperature of 5778 K.

The main exterior features of Cosmo spacecraft are the Multi-Layer Insulation (MLI) and the solar panels. A faithful representation of the MLI material was obtained thanks to a crumpled normal texture⁴ mapped to the spacecraft body for emulating the typical random reflections. The solar arrays have been equipped with a solar cell texture providing base color and displacement, while surface reflection has been obtained through a Blender's glossy shader.

B. Pose Distribution

The distance is randomly selected from a standard normal distribution $N(\mu = 36m, \sigma = 10m)$, rejecting all the values above 70m and below 36m. The x-y offsets on the image plane are uncorrelated random values selected from a multivariate normal distribution, constrained to guarantee that the satellite almost always lies entirely in the image frame. The attitude is randomly sampled from a uniform distribution of rotations in the SO(3) space.

Pose distribution and camera-satellite alignment are governed by the Starfish library [10]. Domain variation is provided through Blender's Python API, by rotating Earth and clouds beneath the satellite before each rendering. Geometrical constraints on the Sun-satellite-Earth angle and Sun-satellite-camera angle are prescribed to avoid dark images due to a non-illuminated camera view. Besides that, lighting direction is randomized across the dataset to provide a comprehensive range of illumination conditions. Sun-tracking rotation of solar panels is added through a Blender "locked track" constraint which allow them to rotate about their longitudinal axis for tracking the Sun direction.

C. Render Setup and Post Processing

A total of 15000 images have been rendered with the PBR Cycles engine through a pinhole camera model. The resolution has been set to 1920x1200 px. Post-processing steps include a glare node, meant to replicate the bloom effect, grayscale conversion, and addition of Gaussian noise and Gaussian blurring to emulate shot noise and depth of field.

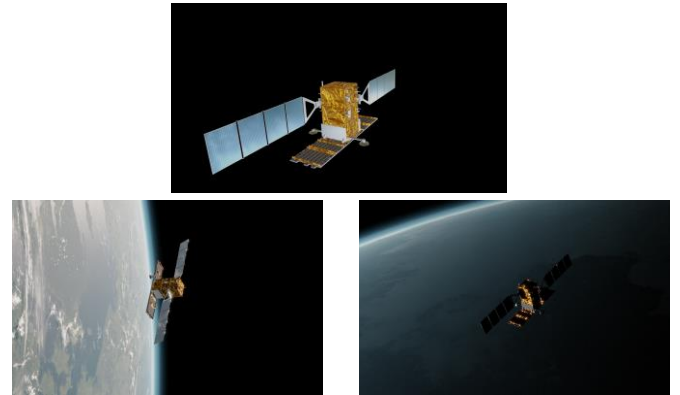


Fig. 1. Close-up preview of the COSMO SkyMed satellite (top), sample images from CPD prior to postprocessing (bottom)

¹ Tom Patterson, www.shadedrelief.com

² NASA, Visible Earth, <https://visibleearth.nasa.gov/>

³ F. Lasse, Physically Correct Atmosphere Shader, <https://gumroad.com/l/JINTt>

⁴ <https://nasa3d.arc.nasa.gov/detail/Sentinel-6>

Fig. 1 reports a close-up render of the satellite and two samples from the dataset, prior to grayscale conversion and noise addition.

III. METHODS

For this work we hold the assumption that the target is known by the chaser, i.e. a wireframe model is available. Since this information was not included in the SPEED dataset, we reconstructed a 3D model through multiview triangulation.

Our pipeline is based on three stages, namely A) spacecraft detection, B) keypoints regression, and C) pose estimation.

A. Spacecraft Detection

Direct processing of high resolution images would prevent real-time inference on low power embedded devices, due to the need of large NNs and a high memory footprint. The purpose of the Satellite Detection Network (SDN) is to identify a Region of Interest (ROI), by detecting the target on the image.

To this end, we employed a Mobiledet Edge TPU optimized model [11] from the TensorFlow (TF) Object Detection API⁵ with an input shape of 320x320 px and about 3.3 millions of parameters. The predicted bounding box is made squared, to avoid distortion, and enlarged by a factor 1.15 to increase the chance that the satellite lies within its margins. The ROI accuracy is defined as the percentage of times the ground truth bounding box is contained within the regressed one. In case the ROI is smaller than the second NN input size, the bounding box is further expanded, otherwise the cropped image is resized to fulfil that requirement.

B. Keypoints Regression

The resulting ROI, possibly corrected to fit within the image edges, is fed into a second CNN which is in charge of detecting a set of predefined keypoints, selected manually from the 3D spacecraft model. We propose a Keypoints Regression Network (KRN) architecture which can be scaled to different accuracy-latency trade-offs. It consists of a fully convolutional model built on top of EfficientNet [12] backbones as well as their lite counterparts⁶, which are obtained removing operations not fully supported by mobile accelerators, and further equipped with a custom regression head. The latter is obtained with a sequence of four convolutions whose details are reported in Table I. The network returns a vector containing normalized coordinates of the landmarks in a pre-defined order.

Model scaling is inherent to the adoption of EfficientNet backbones which are developed to this purpose. Each model features a prescribed combination of network's width, depth, and input resolution. Considering lite and non-lite NNs, both supported by our pipeline, a total of 13 variants is provided.

TABLE I. REGRESSION HEAD STRUCTURE

#	Type	Activation	Kernel size	Padding	#filters
1	Standard	Relu	1	Valid	128
2	Separable	Relu	3	Same	128
3	Standard	-	1	Valid	kpts x2
4	Standard	-	#3 resolution	Valid	kpts x2

However, since at the time of writing EfficientNets are not natively supported by quantization, which is needed to exploit the TPU, we will report results only for the 5 lite versions.

C. Pose Estimation

Target position and orientation are estimated through an EPnP solver [13] with RANSAC exploiting the known 2D-3D correspondences. The resulting pose is eventually refined with a Levenberg–Marquardt (LM) optimization step⁷.

IV. EXPERIMENTS AND RESULTS

A. Training Setup

Both datasets have been divided into train and test clusters through uniform random sampling, as detailed in Table II.

The SDN is trained for 50000 steps with momentum optimizer and Quantization Aware Training (QAT), starting from COCO [14] pretrained checkpoints, applying random crops and horizontal flips to avoid overfitting.

KRNs have been trained with Adam optimizer [15] and mean absolute error loss for 550 epochs on SPEED and 450 epochs on CPD to achieve a similar number of training steps. EfficientNet backbones were initialized with Imagenet [16] checkpoints. Applied augmentations include random image rotations, bounding box enlargements and shifts, random brightness, and contrast adjustments.

The learning rate was gradually reduced according to a cosine decay law after a warmup phase, lasting 2000 steps for the SDN and 10 epochs for the KRNs, where it grows linearly from 0.15 to 0.45 and from 1e-4 to 3e-3 respectively. The batch size was set to 256 for both SDN and KRNs.

The trained networks were first deployed on the CPU of a Coral Dev Board Mini for performance assessment. The results provided in next paragraphs refer to the SPEED dataset, unless otherwise stated.

TABLE II. DATASETS PARTITIONING

Dataset	Train images	Test images
SPEED ^a	9728	2272
CPD	12032	2968

^a We employed only synthetic labeled images from the SPEC competition.

B. Comparison with State of the Art

Even though a direct comparison with other works would require to train and test the NNs on the same images subsets, Table III shows how the error metric attained by all of our pipeline variants are on par with the best ranked submissions at SPEC and later works, with however significantly less NNs parameters.

TABLE III. COMPARISON WITH STATE OF THE ART

Model	E	eq [°]	et [m]	#Parameters
UniAdelaide	0.0094	0.41 ± 1.50	0.032 ± 0.095	176.2 M
Hu, <i>et al.</i> (960px)	0.010	-	-	51.5 M
Our_lite4	0.0119	0.52 ± 0.52	0.034 ± 0.069	15.4 M
Our_lite3	0.0124	0.55 ± 0.53	0.033 ± 0.062	10.5 M
Hu, <i>et al.</i> (640px)	0.013	-	-	51.5 M
Our_lite2	0.0131	0.58 ± 0.57	0.036 ± 0.075	8.4 M
Our_lite1	0.0134	0.59 ± 0.58	0.037 ± 0.068	7.7 M
Our_lite0	0.0149	0.65 ± 0.58	0.040 ± 0.073	6.9 M
EPFL_cvlab	0.0215	0.91 ± 1.29	0.073 ± 0.587	89.2 M
Black, <i>et al.</i>	0.0409	-	-	6.9 M

⁷ https://docs.opencv.org/3.4.12/d9/d0c/group__calib3d.html

⁵ https://github.com/tensorflow/models/blob/master/research/object_detection/g3doc/tf1_detection_zoo.md

⁶ <https://github.com/sebastian-sz/efficientnet-lite-keras>

pedro_fairspace	0.0571	2.49 ± 3.02	0.145 ± 0.239	$\approx 500.0 \text{ M}$
SLAB_baseline	0.0626	2.62 ± 2.90	0.209 ± 1.133	11.2 M

C. From TensorFlow to TensorFlow Lite

As TF is not optimized for on-device inference, we converted all NNs to TensorFlow Lite (TFLite). Performance comparisons are reported in Table IV and Table V, highlighting latency reduction and persistence of accuracy. Note that fps data do not include image loading time from memory.

TABLE IV. SDN PERFORMANCES

SDN	IoU ^a mean	IoU median	ROI accuracy
TF	0.9426	0.9560	96.88 %
TFLite	0.9408	0.9575	97.40 %

^aIoU refers to Intersection over Union.

TABLE V. KRN DETAILS AND TF VS TFLITE PIPELINE PERFORMANCE COMPARISON

KRN	Lite0	Lite1	Lite2	Lite3	Lite4
Input size [px]	224x224	240x240	260x260	280x280	300x300
Pipeline fps TF / TFLite	0.69 / 0.76	0.61 / 0.68	0.56 / 0.62	0.46 / 0.51	0.33 / 0.39
Pose accuracy / TF / TFLite	0.0149 / 0.0150	0.0134 / 0.0136	0.0131 / 0.0131	0.0124 / 0.0126	0.0119 / 0.0118

D. Quantization: CPU vs TPU Inference

Quantization, which is needed for deploying the networks on the TPU, allows decreasing the file sizes up to the 75% thereby significantly reducing latency. Accuracy drop is inevitable; however, to minimize it, KRN have been retrained applying QAT. All networks have been fully quantized except for input and output tensors. A comparison between CPU and TPU inference times is provided in Table VI, highlighting the superior performance of the latter in terms of attainable fps.

TABLE VI. CPU VS TPU INFERENCE TIME

Quantized KRN	Lite0	Lite1	Lite2	Lite3	Lite4
SDN runtime [ms] CPU/TPU	303.54 / 69.82	300.58 / 97.92	296.76 / 128.26	319.60 / 139.39	304.23 / 144.15
KRN runtime [ms] CPU/TPU	136.19 / 36.77	194.29 / 63.26	261.83 / 92.45	425.67 / 177.49	658.96 / 414.77
Pipeline fps CPU/TPU	2.17 / 7.66	1.94 / 5.38	1.72 / 4.06	1.30 / 2.92	1.01 / 1.70
Pose accuracy, E	0.0179	0.0156	0.0151	0.0152	0.0147
Board Temperature [°C]	83.82 / 51.86	84.63 / 51.66	84.80 / 51.43	84.79 / 48.95	85.39 / 46.71

E. Performances on CPD

Finally, we tested our TPU pipelines on the CPD. The good performance of the SDN (Table VII) demonstrates its robustness against variable solar panels orientation. The mean pose accuracy is slightly lower compared to SPEED, as a result of a larger number of outliers (see Table VIII, where the median pose error is instead in line with SPEED). This is primarily due to images where the solar panels occlude a large portion of the SAR antenna, images taken in near eclipse conditions, and those characterized by extreme blooming.

TABLE VII. SDN PERFORMANCES ON CPD

Quantized SDN	IoU mean	IoU median	ROI accuracy
	0.9417	0.9537	99.2 %

TABLE VIII. PIPELINE PERFORMANCES ON CPD

Quantized KRN	Lite0	Lite1	Lite2	Lite3	Lite4
Pose accuracy, E	0.0170	0.0153	0.0159	0.0141	0.0140
Pose accuracy - median	0.0141	0.0129	0.0123	0.0122	0.0114

V. CONCLUSION

Our pipelines perform on par with the state of the art while using extremely lite networks, that can be run real time on low-power embedded hardware. Switching from CPU to TPU architectures allows increasing the fps by a factor of ≈ 2 to 3 (up to 7.7 fps) while reducing the measured power consumption of 25% (from 3W down to 2.2 W). When evaluated on our CPD, the algorithms exhibit accuracies in line with SPEED, although with higher sensitivity to occlusions, which deserves further investigation.

Future developments include testing the NNs on actual space imagery to investigate domain gap.

REFERENCES

- [1] J. Goodwill, G. Crum, J. MacKinnon, C. Brewer, M. Monaghan, T. Wise, and C. Wilson, "NASA SpaceCube Edge TPU SmallSat Card for Autonomous Operations and Onboard Science-Data Analysis," in *2021 AIAA/USU Conference on Small Satellites*, August 2021.
- [2] S. Sharma, C. Beierle, and S. D'Amico, "Pose Estimation for Non-Cooperative Spacecraft Rendezvous Using Convolutional Neural Networks," in *2018 IEEE Aerospace Conference*, pp. 1–12, March 2018.
- [3] S. Sharma and S. D'Amico, "Pose Estimation for Non-Cooperative Rendezvous Using Neural Networks," in *2019 AAS/AIAA Astrodynamics Specialist Conference*, January 2019.
- [4] M. Kisantal, S. Sharma, T. H. Park, D. Izzo, M. Märtens and S. D'Amico, "Satellite Pose Estimation Challenge: Dataset, Competition Design, and Results," in *IEEE Trans. Aerosp. Electron. Syst.*, vol. 56, no. 5, pp. 4083–4098, October 2020.
- [5] B. Chen, J. Cao, A. Parra and T. -J. Chin, "Satellite Pose Estimation with Deep Landmark Regression and Nonlinear Pose Refinement," in *2019 IEEE/CVF International Conference on Computer Vision Workshop*, pp. 2816–2824, October 2019.
- [6] T. H. Park, S. Sharma, and S. D'Amico, "Towards robust learning based pose estimation of noncooperative spacecraft," in *2019 AAS/AIAA Astrodynamics Specialist Conference*, August 2019.
- [7] P. F. Proença and Y. Gao, "Deep Learning for Spacecraft Pose Estimation from Photorealistic Rendering," in *2020 IEEE International Conference on Robotics and Automation*, August 2020.
- [8] K. Black, S. Shankar, D. Fonseka, J. Deutsch, A. Dhir, and M. R. Akella, "Real-Time, Flight-Ready, Non-Cooperative Spacecraft Pose Estimation Using Monocular Imagery," in *31st AAS/AIAA Space Flight Mechanics Meeting*, February 2021.
- [9] Y. Hu, S. Speierer, W. Jakob, P. Fua, and M. Salzmann, "Wide-Depth-Range 6D Object Pose Estimation in Space," in *2021 Conference on Computer Vision and Pattern Recognition*, pp. 15870–15879, June 2021.
- [10] C. Schubert, K. Black, D. Fonseka, A. Dhir, J. Deutsch, N. Dhamani, G. Martin, and M. Akella, "A Pipeline for Vision-Based On-Orbit Proximity Operations Using Deep Learning and Synthetic Imagery," in *2021 IEEE Aerospace Conference*, pp. 1–15, March 2021.
- [11] Y. Xiong, H. Liu, S. Gupta, B. Akin, G. Bender, Y. Wang, P.-J. Kindermans, M. Tan, V. Singh, and B. Chen, "MobileDets: Searching for Object Detection Architectures for Mobile Accelerators," in *2021 IEEE/CVF Conference on Computer Vision and Pattern Recognition*, pp. 3824–3833, June 2021.
- [12] M. Tan and Q. Le, "EfficientNet: Rethinking Model Scaling for Convolutional Neural Networks," in *International Conference on Machine Learning*, pp. 6105–6114, June 2019.
- [13] V. Lepetit, F. Moreno-Noguer, and P. Fua, "EPnP: an accurate $O(n)$ solution to the PnP problem," in *International Journal of Computer Vision*, vol. 81, no. 2, pp. 155–166, February 2009.
- [14] T.-Y. Lin, M. Maire, S. J. Belongie, L. D. Bourdev, R. B. Girshick, J. Hays, P. Perona, D. Ramanan, P. Doll'ar, and C. L. Zitnick, "Microsoft COCO: Common objects in context," in *13th European Conference on Computer Vision*, September 2014.
- [15] D. P. Kingma and J. Ba, "Adam: A Method for Stochastic Optimization," in *3rd International Conference on Learning Representations*, May 2015.
- [16] A. Krizhevsky, I. Sutskever, and G. E. Hinton, "ImageNet classification with deep convolutional neural networks," in *Advances in Neural Information Processing Systems*, vol. 25, pp. 1106–1114, 2012.